Available online at www.sciencedirect.com
ScienceDirect
International Journal of Heat and Mass Transfer 51 (2008) 457–468
International Journal of HEAT and MASS TRANSFER
www.elsevier.com/locate/ijhmt

Heat transfer and pressure drop in rectangular channel with compound roughness of V-shaped ribs and deepened scales

S.W. Chang [a,*], T.-M. Liou [b], K.F. Chiang [c], G.F. Hong [d]

[a] Thermal Fluids Laboratory, Department of Marine Engineering, National Kaohsiung Marine University, No. 142, Haijhuan Rd., Nanzih District, Kaohsiung 811, Taiwan, ROC
[b] Department of Power Mechanical Engineering, National Tsing Hua University, Hsinchu, Taiwan, ROC
[c] Department of Research and Development, Asia Vital Components Co., Ltd., 7F-3, No. 24, Wu-Chuan 2Rd., Hsin Chuang City, Taipei, Taiwan, ROC
[d] Department of Marine Engineering, National Kaohsiung Marine University, Taiwan, ROC

Received 22 November 2006; received in revised form 21 May 2007
Available online 26 July 2007

Abstract

A novel heat transfer enhancement (HTE) roughness with V-shaped ribs and deepened scales is devised. Performances of heat transfer and pressure drop in a rectangular channel fitted with such HTE surfaces are experimentally examined for both forward and backward flows in the *Re* range of 1000–30000. Relative to the smooth-walled pipe flow conditions, HTE ratios for the present test channel with forward and backward flows, respectively, reach 9.5–13.6 and 9–12.3 for laminar flows and 6.8–6.3 and 5.7–4.3 for turbulent flows. Comparisons of heat transfer data, pressure-drop measurements and thermal performance factors with previous results collected from varieties of HTE devices demonstrate the superiorities of this compound HTE device. The decrease of HTE ratio as *Re* increases for turbulent flows, which is a common setback for several HTE elements, is almost diminished in the channel fitted with present compound HTE surfaces. Experimental correlations of heat transfer and friction coefficient for the tested channel with forward and backward flows are derived for design applications.

Keywords: Compound V-ribs and scaled roughness; Heat transfer augmentation

1. Introduction

Methods of passive heat transfer enhancement (HTE) have been extensively explored with the attempts to overcome the thermal problems subject to high heat fluxes. A variety of surface ribs [1–6], dimples [7–9], pin-fins [10,11], perforated baffles [12], twisted tapes [13–16], winglet-type vortex generators [17,18] and the scaled roughness [19] has been devised to enhance heat transfer rates in ducts. Mechanisms for heat transfer augmentation vary with different HTE elements [1–19] that generally elevate heat transfer rates for turbulent flows as much as 200–450%. The flow physics for heat transfer improvements in ribbed channels include the periodical penetration of protruding ribs across boundary layers, turbulence promotions and the generation of large scale secondary flows. The cross stream vortices induced by angled ribs convey the cooler fluid from the duct core towards the heated surface that augment heat transfer further by diminishing the thickness of hydrodynamic and thermal boundary layers. Depending on the configurations of rib floor and channel geometry [1–6], HTE ratios in ribbed channels vary between 2 and 3.5 times of the Dittus–Boelter references [20]. Thermal performances of rib-roughened surfaces are generally impaired by increasing *Re* or decreasing the channel height-to-width (H/W) ratio [1–6]. For the channel with H/W ratio of 1/4, the pressure drops are about 8–16 times of the square-channel level if the same HTE ratio is to be achieved [4].

Flow structures produced by the dimpled surface are characterized by vortex pairs those periodically shed from

* Corresponding author. Tel.: +886 78100888x5216; fax: +886 5712219.
E-mail address: swchang@mail.nkmu.edu.tw (S.W. Chang).

0017-9310/$ - see front matter © 2007 Elsevier Ltd. All rights reserved.
doi:10.1016/j.ijheatmasstransfer.2007.05.010

Nomenclature

English symbols

D	diameter of scale (m)
d	hydraulic diameter of the test channel (m)
e	height of rib or scale (m)
C_f	fanning friction factor $= [\Delta P/(0.5\rho W_m^2)]/(d/4L)$
$C_{f\infty}$	fanning friction factor for developed flow in smooth walled plain tube
H	channel height (m)
k_f	thermal conductivity of fluid (W m^{-1} K^{-1})
L	channel length (m)
l^R	rib land (m)
Nu	average Nusselt number at each axial location $= qd/k_f(T_w - T_b)$
$\overline{Nu}$	averaged Nusselt number for developed flow
Nu_∞	Nusselt number value for developed flow in smooth walled plain tube
P	pitch of rib or scale (m)
ΔP	pressure difference between two pressure taps (N m^{-2})
q	convective heat flux (W m^{-2})
Re	Reynolds number $= \rho W_m d/\mu$
T_b	fluid bulk temperature (K)
T_w	wall temperature (K)
W	channel width
W_m	mean flow velocity (m s^{-1})
x	axial location referred to flow entry as origin (m)
X	dimensionless axial location (x/d)

Greek symbols

α	attack angle of rib or scale (°)
ρ	density of fluid (kg m^{-3})
μ	fluid dynamic viscosity (kg m^{-1} s^{-1})
η	thermal performance factor $= (\overline{Nu}/Nu_\infty)/(C_f/C_{f_\infty})^{1/3}$

Superscripts

R	rib
S	scale

each dimple. A distinct up-wash region and packets of fluid emanating from the central region of each dimple develop in the region near the dimple diagonals. Vortex pairs in the dimpled channel often appear in the form of collections of stretched vortex pairs as they advect downstream [7]. Local heat transfer enhancements are more pronounced near the downstream rims of dimples. The periodicity of vortex shedding events in the dimpled channel becomes more furious as the channel H/W ratio decreases so that the more pronounced heat transfer augmentation near the downstream rim of each dimple [9] is produced. However, unlike the secondary flows induced by angled ribs, the strong and continuous vortical cells cannot be established over the cross-section of the dimpled channel. Spatially averaged Nusselt numbers in dimpled channels generally fall between 1.85 and 2.89 times of the smooth wall levels [7].

Channels with pin-fin array are widely adopted as the cooling passages near the trailing edge of a gas turbine blade where higher levels of heat transfer augmentation are requested but the penalty of high pressure drops is tolerated. Horseshoe vortices are initiated at locations immediate upstream of individual pins. Two primary vortex pairs downstream of each pin row are formed by the blockage and streamline displacement effects of the pin-fins, which are the remnants of the two legs of the horseshoe vortices. As the structural evolution for such primary vortex pair is a dynamic process, the HTE mechanism is added by promoting the secondary advection between fluids and the turbulence level [11]. In addition to the fin effects offered by a large number of pins, HTE ratios in the pin-fin channels are in the range of 2–3 [10,11]. A recent device of perforated baffles combines the effects of ribs, fins and impingement for heat transfer augmentation. The inclined perforated baffles act as fins to induce large scale vortices with enhanced turbulent activities and fluid mixing. Each inclined perforated baffle contains circular holes through which the impinging jets are produced and directed toward the heated surface. In the channel with two opposite walls roughened by inclined perforated baffles [11], the averaged Nusselt numbers for turbulent flows were raised to the levels about 2–5 times of the Dittus–Boelter references. However, in despite of its drawbacks for structure integrities and manufacturing difficulties, the HTE performances for perforated baffles under fouling conditions can be significantly impaired if the orifices through the perforated baffles are blocked to prohibit jet impingements.

Twisted tapes in ducts provide considerable HTE effects with reasonable pressure drop penalty which are also suitable for retrofit applications. Longitudinal swirls and the modification of near wall velocity profile due to the various vorticity distributions in the vortex core are two major attributes for HTE effects. Additional HTE mechanisms for twisted tape inserts include the partitioning and partial blockage of ducted flow, fin effects and the elongated twisted flow path [13–16]. Impacts of such HTE measure remain very effective for laminar flows but fall dramatically for turbulent flows as the lateral fluid mixings promoted by twisted tapes are well preserved in turbulent structures. HTE ratios in tubes with twisted tape inserts could be, respectively, raised to 30 and 3.5 times of the plain tube levels for laminar and turbulent flows [14]. Winglet-type longitudinal vortex generators [17,18] offer considerable heat transfer elevations with significant pressure losses in channels. The longitudinal vortices are generated along the side edges of vortex generators (VG) due to flow separations at leading edges of VG as a result of pressure differences

between the upstream and downstream sides of each VG. These VG-induced vortices swirl the bulk flow that promote fluid mixings close to and far from the channel walls that generates considerable heat transfer augmentations [17]. But the large cost of pressure loss in VG channel prevents its wide applications and has led to an alternative approach by fitting VG on one wall with the rib floor on the opposite wall [18]. HTE ratios of a VG channel from the smooth-walled references are in the ranges of 2.9–3.41 for turbulent flows [18]. In view of preserving the structural stiffness and integrity of a coolant channel, the scale-roughened surface is proposed [19]. A large amount of deepened scales over the roughened wall breaks the boundary layers and promotes turbulence activities. Localized vortical flow cells are triggered when the bulk flow traverses each scale either from the forward or backward direction. Nusselt number ratios (Nu/Nu_∞) for laminar forward and backward flows in the scale-roughened channel of $H/W = 1/8$ were in the range of 7.4–9.2 and 6.2–7.4, respectively. Turbulent heat transfer rates in the scale-roughened narrow channel were about 4.5 and 3 times of the Dittus–Boelter levels for the forward and backward flows, respectively [19].

The on-going search for better heat transfer performances is continued by combining different HTE elements into a compound HTE device. The so called compound enhancement generally offers the higher HTE ratio than the individual techniques applied separately. Research goals in this respect involve the further elevations of HTE ratio and thermal performance factor with the extended effective *Re* range. Typical examples of such compound HTE measures for channel flows include the combination of twisted tape and corrugated tube [21] and the serrated twisted tape [22]. The corrugated tube with twisted tape insert could elevate Nusselt numbers to 1.9–9.6 times of the plain tube value in the *Re* range of 4000–60,000 [21]. Insertion of rib-roughened twisted tape in a tube with $5000 \leqslant Re \leqslant 25{,}000$ acquires the HTE ratios of 2.5–4.8 times of the plain tube value [22]. Compound techniques have become the frontier area of enhancement that proves promise for a variety of practical applications. Following on our previous work [19] that examined the thermal performances of the scaled roughness, this study was motivated by the need to further elevate HTE ratios for the coolant passages in a gas turbine blade. Blade cooling applications require the considerations of structural integrities of HTE devices and the cost and availability of fabrication means. The present experimental study examines the HTE ratios, pressure drop characteristics and the thermal performance factors for a novel compound technique that combines the scaled roughness and V-shaped ribs to form an effective element of surface roughness. With turbine blade cooling applications, requirements for structural integrities of HTE device itself are satisfied by the present compound HTE surface. There is no previous study available for this novel surface invented from our Thermal Fluids Laboratory.

2. Experimental details

2.1. Apparatus

Fig. 1 depicts the experimental apparatus that shows the schematics of test assembly (a) and the geometrical details of compound V-ribs and scale roughness (b). As shown in Fig. 1a, the IWATA SC-175C screw-type compressor (1) and the refrigerating unit (2) continuously fed the dehumidified and cooled airflow to the test assembly at the ambient temperature level. The test airflow was then channeled through a set of pressure regulator and filter (3) with the mass flow rate measured and adjusted by the Bronkhorst mass flow meter (4) and the needle valve (5), respectively. The pressure transducer (6) with digital display detected the entry pressure of coolant flow. Prior to entering the rectangular test section with two opposite walls roughened by compound V-ribs and scales (7), the pressurized airflow entered a 150 mm × 150 mm × 80 mm plenum chamber (8). The cross-sectional area ratio between the plenum chamber and the test channel was 3.75 that simulated the abrupt entry condition. Dimensions of the test channel were 80 mm × 40 mm × 220 mm. Channel aspect ratio (H/W) and hydraulic diameter are 1/2 and 53 mm, respectively. A K-type thermocouple penetrated into the core of plenum chamber adjacent to the entrance of test channel to measure the coolant entry temperature. This fluid entry temperature was selected to define the fluid properties at the flow entrance for the evaluation of Reynolds and Prandtl numbers at the flow entrance. Streamwise increments of flow bulk temperature (T_b) from one measurement spot to its successive downstream location were determined using the sequential energy balance method. This method determined T_b values at the axial locations where wall temperatures (T_w) were detected. At the exit plane of the heated test section, three type K thermocouples with equal spanwise interval penetrated into the core of the converging section (9) to measure the fluid temperatures. The exit temperature of fluid was obtained by averaging the three thermocouple measurements. To check for the accuracy of energy conservation at the stage of data acquisition, the evaluated T_b value was constantly checked with the measured fluid exit temperature. Data batch was accepted when the differences between the measured and calculated T_b values were less than 8% at the exit plane.

Structural consolidations of V-ribs and scales over each roughened heat transfer surface are depicted in Fig. 1b. The V-ribs on two opposite heated walls were arranged in the staggered manner with the following geometrical definitions for the rib configurations:

Rib angle of attack, α^R, = 45°;
Rib height, e^R (1.77 mm)/channel height, H (40 mm) = 0.04;
Rib pitch, P^R (17.7 mm)/rib height, e^R (1.77 mm) = 10;
Rib land, l^R (1.77 mm)/rib height, e^R (1.77 mm) = 1.

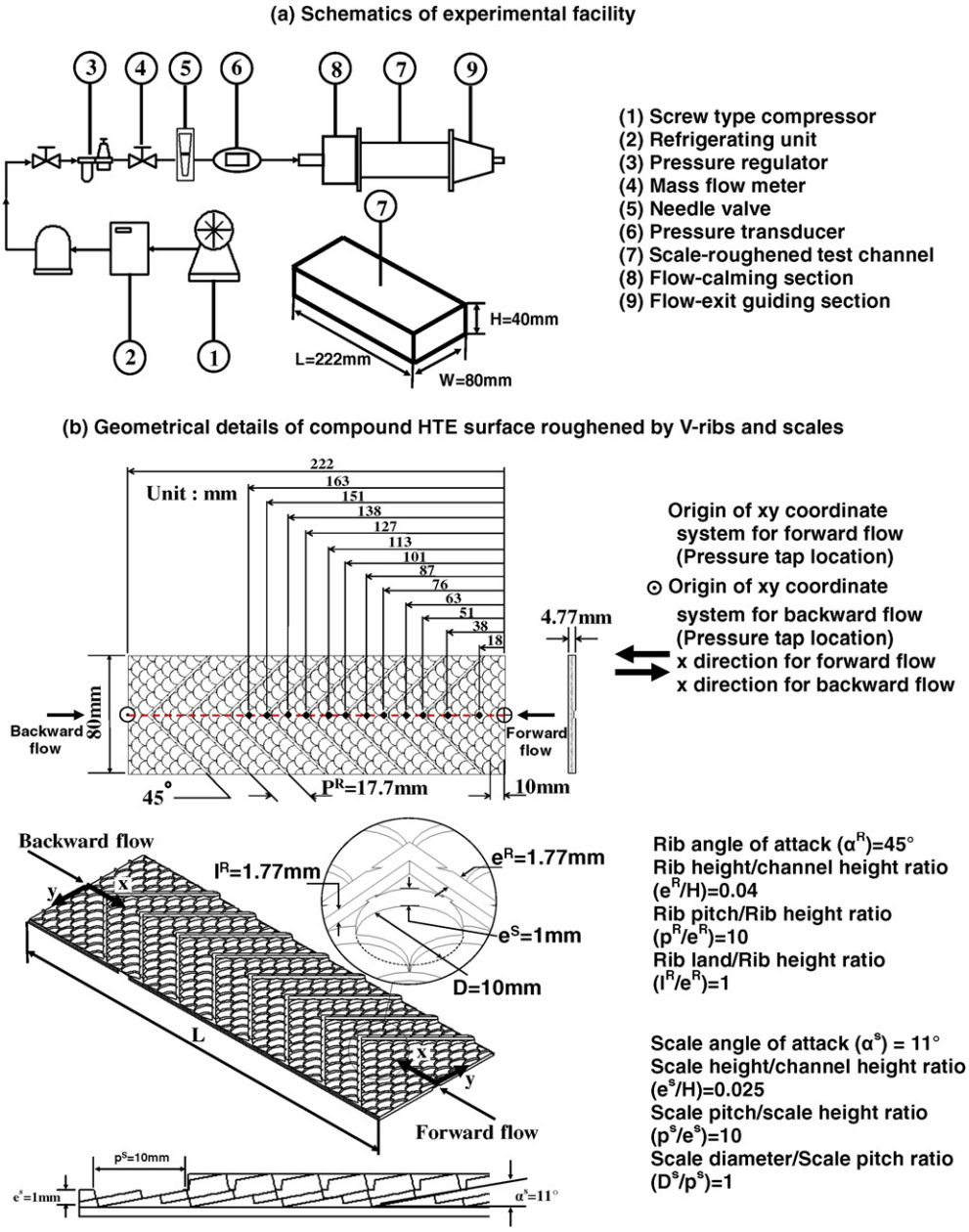

Fig. 1. Experimental apparatus: (a) schematics of experimental facility and (b) geometrical details of compound HTE surface roughened by V-ribs and scales.

The surface scales were deepened into each scale-roughened surface between two adjacent V-ribs. These scales were arranged in the staggered manner on each roughened heat transfer surface as depicted in Fig. 1b. Geometrical descriptions of the scaled surface are specified in terms of four non-dimensional parameters of

Scale angle of penetration (α^S) = 11°;
Scale height, e^S (1 mm)/channel height, H (40 mm) = 0.025;
Scale pitch, P^S (10 mm)/scale height, e^S (1 mm) = 10;
Scale diameter, D^S (10 mm)/scale pitch, P^S (10 mm) = 1.

The two opposite wide walls of test channel fitted with the compound V-ribs and scaled surfaces were machined from two stainless steel plates with the thermal conductivity of 15 W m^{-1} K^{-1} and electrically heated by two 0.5 mm thick Minco thermal foils. Each heating foil was sandwiched between a 25 mm thick Teflon plate and the roughened heat transfer surface which generated the basically uniform heat flux heating condition. The Minco thermal foil is attached to the back flat surface of each roughened steel plate by the forces generated from a series of axial bolts along the test channel. Because the ribs and scales are machined from the same stainless steel material of high

conductivity, the *Nu* data generated by the present study represents the average Nusselt number at each axial location. As indicated in Fig. 1b, 12 K-type thermocouples with equal interval were installed on the back face of along the centerline the roughened surface for wall-temperature measurements. These thermocouple locations for T_w measurements corresponded to the rib and mid-rib locations. All the temperature measurements were monitored and stored in a PC using through the data logger for the subsequent data processing. Wall temperature measurements at all the axial locations were corrected into the base-line surface as indicated in Fig. 1b using the one dimensional heat conduction equation. The origins of streamwise (x) and spanwise (y) coordinate systems for the forward and backward flows were selected at the middle span of each entry edge. Thermal insulation material was wrapped over the outer surface of the test channel to minimize the external heat loss. Via the heat loss calibration tests, it was found that the external-heat loss over the heat transfer surface increased with the increase of wall-to-ambient temperature difference. As the wall temperatures over the roughened surface were not uniformly distributed, local heat loss fluxes varied spatially. With a uniform heat flux supplied from the Minco thermal foil, the convective heat flux over the heat transfer surface was not perfectly uniform. Axial distributions of convective heat flux were obtained by subtracting the local heat loss flux from the total heat flux supplied. A review for the entire data of convective heat flux revealed that the non-uniformities in heat flux distributions were less than 9.1% due to the small amount of external heat loss. Therefore, the basically uniform heat flux heating condition was simulated by the present test rig.

Measurements of pressure drop were performed separately at isothermal conditions. To measure the pressure drop across the test channel at each predefined Reynolds number, two flexible tubes were equipped with pressure taps of 0.5 mm diameter at two origins of the coordinate systems specified in Fig. 1b. A short 1 mm diameter stainless steel tube was glued on the top of each pressure tapping to connect the flexible tube. Pressure differences between these two taps were metered by a digital type micromanometer with precision of 0.001 mm-H_2O. This arrangement for pressure-drop measurements absorbed the friction loss in the developing flow region. As a part of the coolant flow inside a gas turbine blade was under developing, the present arrangement for pressure-drop measurements offered the overall assessments for the flow resistance over the entire test channel, which generated the higher levels of pressure drop than those acquired from the developed flow regime.

2.2. Program and data processing

Heat transfer and pressure drop tests were performed with the airflows directed in the forward and backward directions at $Re = 1000$, 1500, 2000, 5000, 10,000, 15,000, 20,000, 25,000 and 30,000. This tested *Re* range covered both laminar and turbulent flows. Streamwise heat transfer variations along the centerline of the roughened surface and pressure drops across the test channel at various Reynolds numbers were examined. As the top face of each scale was deepened into the heated wall with an inclined angle (α^S) and the V-ribs were pointed in the downstream direction, performances of heat transfer and pressure drop in the test channel were affected by the direction of flow. Influences of *Re* and flow direction on the local and spatially averaged heat transfers, the pressure drops and the thermal performance factors were analyzed for this particular test channel roughened by the compound V-ribs and scales. The HTE ratios, friction augmentations and thermal performance factors between the present test channel and those collected from a variety of enhanced channels were compared to highlight the superiority of present compound HTE technique. Empirical correlations that evaluated the spatially averaged heat transfer rates and the overall friction coefficients in the present test channel at both forward and backward flow conditions were generated for design applications.

Heat transfer measurements were performed under steady-state conditions. The steady state was assumed when the variations of local wall temperatures with several successive scans were less than 0.3°C. The elapsed time to achieve the steady state generally took 30 min after the heating power or flow rate was adjusted. The various heat fluxes fed into the heating foil affected the Reynolds number at the flow entrance even if the airflow rate remained invariant due to the thermal impact on fluid properties. After the adequate adjustment of coolant mass flow rate to compensate the thermal impact on *Re* value, maximum variations in Reynolds number at the entry plane of test channel were controlled within ±1% deviation from the targeting value. Reynolds number (*Re*) and local Nusselt number (*Nu*) were experimentally defined using Eqs. (1) and (2), respectively,

$$Re = \rho W_m d/\mu \tag{1}$$

$$Nu = qd/[k_f(T_w - T_b)] \tag{2}$$

The symbols of ρ, W_m, d and μ in Eq. (1) are the fluid density, bulk mean flow velocity, hydraulic-diameter of test channel and viscosity of fluid, respectively. The local convective heat flux (q) in Eq. (2) was obtained by subtracting the local heat loss flux from the supplied heat flux over the electrical heating foil. The heating surface adopted to evaluate the supplied and lost heat fluxes was the projected area of the V-ribs and scales. Having determined the local convective heat flux, the local Nusselt number (*Nu*) was defined using Eq. (1). All the fluid properties appeared in Eqs. (1) (2) were evaluated from the local flow bulk temperature, T_b.

Dimensionless pressure drops over the test channel were evaluated as the Fanning friction factors (C_f) using the pressure drops (ΔP) across the test channel of length L with mean flow velocity (W_m) as

$$C_f = [\Delta P/(0.5\rho W_m^2)]/(d/4L) \tag{3}$$

Uncertainties of temperature measurements were the major sources to attribute the uncertainties of coolant's thermal conductivity, fluid density and viscosity. The maximum uncertainties associated with Nu and Re and C_f were, respectively, estimated as 10.2% and 4.8% and 2.1% following the policy of ASME on reporting the uncertainties in experimental measurements and results [23].

References to assess HTE ratios and pressure-drop augmentations in the present test channel were selected as the levels in smooth circular tube with fully developed flow. The reference Nusselt number (Nu_∞) and friction factor ($C_{f\infty}$) for laminar and turbulent developed flows are defined in the following equations:

$$Nu_\infty = 48/11 \quad \text{(laminar pipe flow with uniform heat flux)} \tag{4}$$

$$C_{f\infty} = 16/Re \quad \text{(laminar pipe flow)} \tag{5}$$

$$Nu_\infty = 0.023Re^{0.8}Pr^{0.4} \quad \text{(Dittus–Boelter correlation for turbulent flow)} \tag{6}$$

$$C_{f\infty} = 0.079Re^{-0.25} \quad \text{(Blasius equation for turbulent flow)} \tag{7}$$

Thermal performance factors (η) for the present test channel based on the constant pumping power consumptions are quantified using the following equations:

$$\eta = (\overline{Nu}/Nu_\infty)/(C_f/C_{f\infty})^{1/3} \tag{8}$$

3. Results and discussion

3.1. Heat transfer measurements and correlations

Fig. 2 compares the axial Nu distributions along the centerline of roughened heat transfer surface at each Re tested between forward and backward flows. The axial Nu profiles follow a general trend of exponential decay subject to minor zig-zag Nu variations triggered by V-ribs. The abrupt entrance of present test channel generates developing flows in the axial spans about $0 < x/d < 1.58$ and $0 < x/d < 2.72$ for forward and backward flows, respectively. As the rib-wise secondary flows induced by V-ribs also traverse the deepened scales, Nu distributions over the present HTE surface are modified from those over the smooth-walled rib floors [1,2,5]. In this respect, although the zig-zag Nu profile triggered by V-ribs is observed with lower Nu values at rib locations, the amplitudes of zig-zag oscillations in the developed flow region are significantly moderated from the results obtained with smooth-walled rib floors [1,2,5]. The suppression of rib induced zig-zag Nu variations due to the presence of surface scales features a merit for turbine blade cooling applications. The lower Nu values shown at rib locations are consistent with the experimental results detected from the thermocouple measurements [1] for which the surface ribs act as the additional thermal barriers when the heat flux is issued from the heating foil toward the bulk flow. It is impractical to correct the thermocouple measurements at rib locations toward their rib-tops without the knowledge of convective heat transfer coefficients over all three faces of each V-rib. As a result, the subsequent data analysis discards the heat transfer results detected from the rib locations.

A conceptual description of flow mechanics in the scale-roughened narrow rectangular channel with forward and backward flows has been previously proposed [19] which pointed out the subtle differences in flow structures between the forward and backward flows. The forward bulk stream initially traverses the protruding circular rims of scales that trigger a large number of three dimensional vortical cells. After the flow stream traversing these protruding circular rims that encounters the downhill faces of scales, the similar flow mechanisms developed in the dimpled channel with the up-wash packets of fluid emanating from the deepened scales are likely to be produced. The backward flow initially encounters the scale-shaped cavities before traversing the protruding circular rim of each scale. Vortical cells are generated that advect further downstream. The inclined surface of each scale is in the uphill direction that lifts these vortical cells off the heating surface toward the channel core. As seen in Fig. 2, differences in the flow structures between forward and backward flows result in different heat transfer performances even if the agitated and secondary flows persist in the present channel roughened by scales and V-ribs. It is expected that the interactive V-rib and scale induced flow phenomena alter the spanwise as well as the streamwise heat transfer distributions and the effects of forward and backward flows on the spatial heat transfer distributions also deviate from our previous study [19] to some extends due to the presence of V-ribs. For the channel fitted with V-ribs, the high heat transfer regions appear near the side regions of forward flow, and at the center in case of backward flow due to the orientation of the present V-ribs. Although this V-rib induced heat transfer characteristic exists, the heat transfer coefficients with forward flow are consistently higher than those of backward flows due to the different scale geometries encountered by the traversing flow. Heat transfer differences between the forward and backward flows continuously increase as Re increases with the higher heat transfer coefficients constantly developed for the forward flows.

In addition to the vortical flow structures contributing to heat transfer augmentations, the deepened scales arranged in the staggered manner between two adjacent V-ribs are conjoint to form a large numbers of step-by-step protruding circular fronts that keep breaking the boundary layers over the roughened heat transfer surface. Activities of vortical flows are enhanced by these deepened circular scales that augment vorticity and turbulence levels with the increased friction-loss penalty. Strong cross-stream secondary flows are simultaneously induced by the protruding V-ribs that sweep the highly turbulent vortical cells from these deepened scales toward the channel core for heat exchanges via furious fluid mixings. These compound

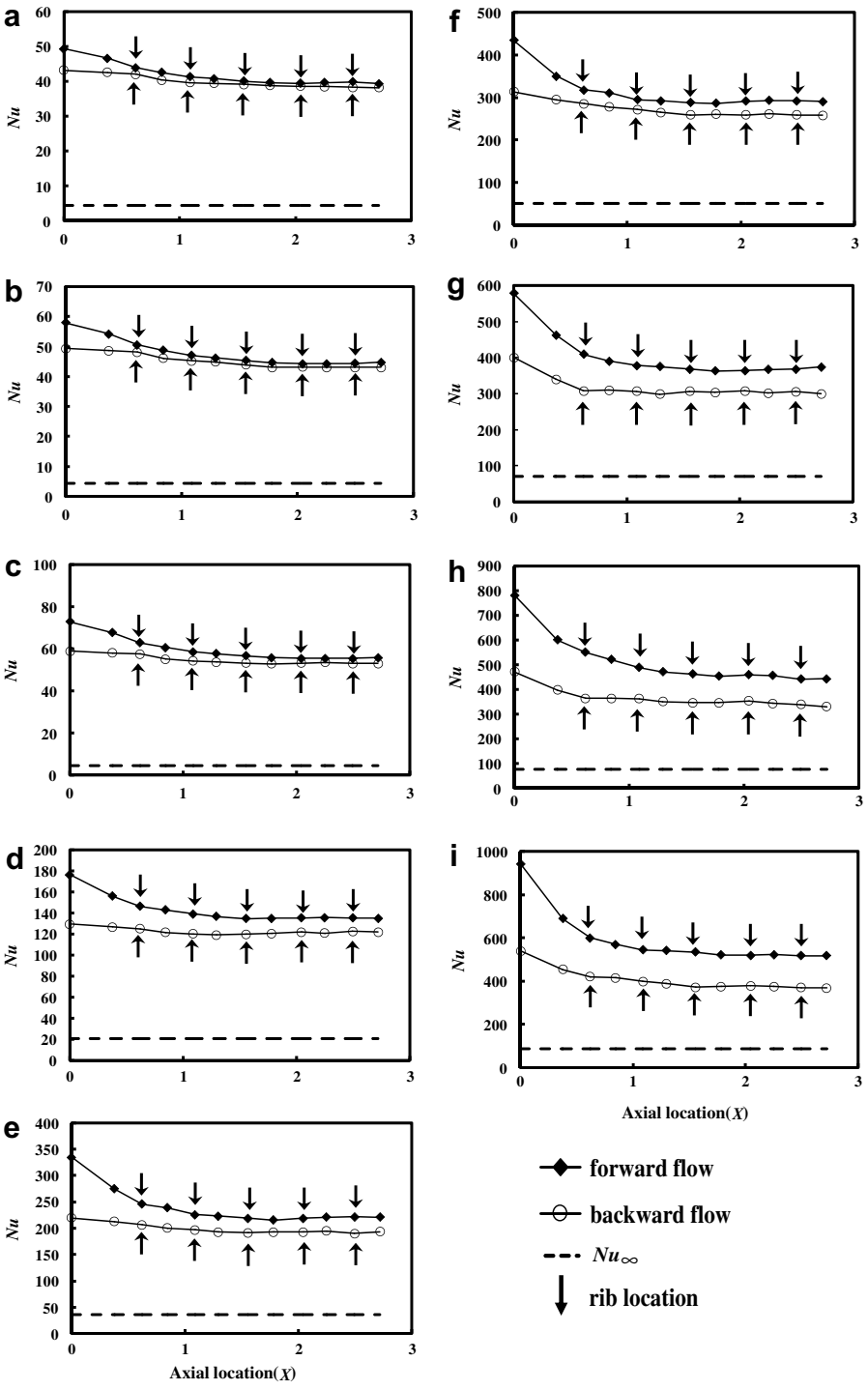

Fig. 2. Axial distributions of Nusselt number for forward and backward flows in rectangular channel roughened by compound V-ribs and scales at Reynolds numbers of: (a) 1000, (b) 1500, (c) 2000, (d) 5000, (e) 10,000, (f) 15,000, (g) 20,000, (h) 25,000 and (i) 30,000.

mechanisms of boundary layer breaking, enhancements of turbulent and vortical activities and the strong cross-stream secondary flows induced by V-ribs simultaneously interact to generate significant heat transfer augmentations. This is demonstrated in each plot of Fig. 2 by comparing the present heat transfer levels with the Nu_∞ references. Turbulent Nusselt numbers in the developed flow regimes at Reynolds number of 30,000 are elevated to the levels about 6.8 and 6.3 times of the Nu_∞ references for forward and backward flows, respectively, which offer the very high HTE ratios for turbulent flows.

A common setback for a variety of HTE devices to augment turbulent heat transfer is the decreased HTE ratios as *Re* increases. The complex flow structures generated in the test channel fitted with the present HTE surfaces involve the enhanced turbulence intensities and the furious vortical

mixings due to the presence of surface scales. These scale-triggered flow phenomena tend to be augmented by increasing *Re* which consequently enhances the dependency of *Nu* on *Re*. Such weighted *Re* impact on *Nu* extends the effective *Re* range for HTE. This has been demonstrated by our previous study that showed the local Nusselt numbers in a channel fitted with scaled roughness were, respectively, correlated by $Re^{0.815}$ and $Re^{0.7}$ for forward and backward flows so that the effective *Re* range for turbulent heat transfer augmentations were considerably extended [19]. For the present test channel, heat transfer results in the developed flow regime are analyzed to reveal the functional relationship between Nusselt and Reynolds numbers through which the heat transfer correlations for the forward and backward flows are also revealed. Initially, the Nusselt number value of developed flow in the present test channel ($\overline{Nu}$) is obtained by averaging the local *Nu* data collected at all the mid-rib locations in the developed flow region. Fig. 3 depicts the varying manners of $\overline{Nu}$ versus *Re* for forward and backward flows. The referenced Nusselt numbers (Nu_∞) for laminar and turbulent flows over the tested *Re* range are included in Fig. 3 for comparisons. Two sets of $\overline{Nu}$ data trends shown in Fig. 3 are well correlated by Eqs. (9) and (10) for the forward and backward flows, respectively,

$$\overline{Nu} = 0.157 \times Re^{0.787} \quad \text{(forward flow)} \tag{9}$$

$$\overline{Nu} = 0.49 \times Re^{0.649} \quad \text{(backward flow)} \tag{10}$$

In the range of $1000 \leqslant Re \leqslant 30{,}000$, 96% of the present experimental Nusselt numbers ($\overline{Nu}$) agree within ±10% discrepancies from the predictions of Eqs. (9) and (10). As the Prandtl number effects are absorbed into the coefficients of Eqs. (9) and (10), which are not included as a parametric effect when these correlations are developed, Eqs. (9) and (10) are essentially limited to dry air. It is interesting to note in Figs. 2 and 3 that the heat transfer differences between the forward and backward flow conditions increase as *Re* increases. This particular result indicates that the flow interactions triggered by V-ribs and scales are different between the forward and backward flows. The deepened scales possibly disturb the secondary flows induced by V-ribs in case of backward flow so that the differences in compound heat transfer augmentations between forward and backward flows systematically increase as *Re* increases.

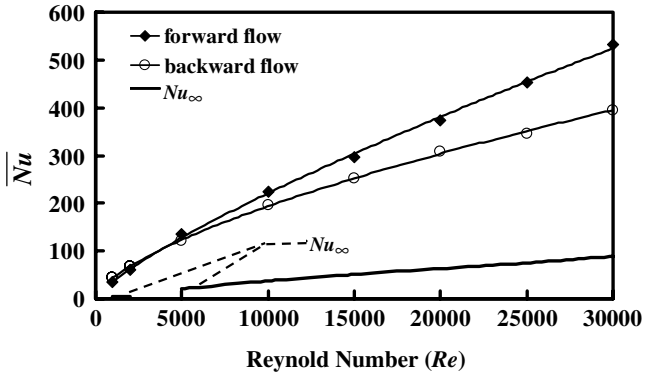

Fig. 3. Variations of developed-flow Nusselt number against *Re* for forward and backward flows in rectangular channel roughened by compound V-ribs and scales.

The *Re* exponents for the forward and backward flows in the present test channel are reduced from those obtained with the scale-roughened channel of 0.815 and 0.7 [19] due to the presence of V-ribs. However, the *Re* exponents of 0.787 and 0.649 shown in Eqs. (9) and (10) are both elevated from the typical range of 0.5–0.6 for the rib-roughened channels with smooth surfaces between ribs [1–5]. As the *Re* exponent of 0.787 for the forward flow in present test channel is very close to 0.8 in the Dittus–Boelter correlation, the *Re* range offering the higher ratios of $\overline{Nu}/Nu_\infty$ is considerably extended. This result is particularly useful for turbine blade cooling applications in which the operational Reynolds numbers are often above than 30,000.

The HTE impacts of present compound roughness are evaluated as the Nusselt number ratios in terms of $\overline{Nu}/Nu_\infty$. As the Nu_∞ references selected for laminar and turbulent flows are different, two different patterns of $\overline{Nu}/Nu_\infty$ versus *Re* for laminar and turbulent flows are observed in Fig. 4 with either forward or backward flow. Also compared in Fig. 4 are the HTE ratios reported from different research groups using varieties of HTE devices [1–19,21,22]. With $Re < 3000$, $\overline{Nu}/Nu_\infty$ ratios increase with the increase of *Re* which, respectively, fall in the range of 9.5–13.6 and 9–12.3 for the forward and backward laminar flows. With developed turbulent flows of $5000 \leqslant Re \leqslant 30{,}000$, $\overline{Nu}/Nu_\infty$ ratios decrease with the increase of *Re* in the present test channel. The different decreasing rates of $\overline{Nu}/Nu_\infty$ ratios versus *Re* between turbulent forward and backward flows as indicated in Fig. 3 reflect a result of different *Re* exponents in Eqs. (9) and (10). The decreasing rate of $\overline{Nu}/Nu_\infty$ ratios for the present forward turbulent flow depicted in Fig. 4 is almost indistinguishable which demonstrates the superiority of the present compound roughness from the comparative groups [1–18,21,22] in the respect of extending the effective *Re* range for HTE. Moreover, the present compound roughness with forward turbulent flow reaches the highest $\overline{Nu}/Nu_\infty$ ratios in the range of 6.8–6.3 among all the comparative groups collected in Fig. 4. Nevertheless, in the present test channel with backward turbulent flow, the $\overline{Nu}/Nu_\infty$ ratios vary in the range of 5.7–4.8 over the range of $5000 \leqslant Re \leqslant 30{,}000$ which are still comparable with the HTE effects offered by several compound HTE techniques [12,21,22].

3.2. Pressure-drop measurements and correlations

Fig. 5a and b, respectively, plots fanning friction factors (C_f) and $C_f/C_{f\infty}$ ratios against *Re* for the forward and backward flows. The present Fanning friction factor is calculated from the pressure drop across the entire length of test channel. As *Re* increases, the Fanning frictions factors decrease toward the asymptotic values for both forward and backward flows in present test channel as shown in

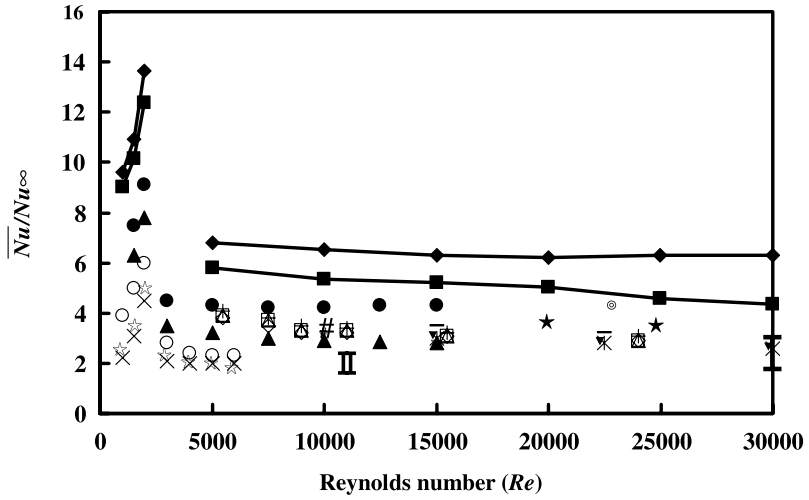

Symbols	References	Channel aspect ratio	α^R	Pitch ratio	e/H	HTE device
◆	Forward flow (present study)	2	45	10	0.044	V-rib Scaled surface
■	backward flow(present study)	2	45	10	0.044	V-rib Scaled surface
▼	Han et al. 45deg V-up[1]	1	45	10	0.0625	Continuous rib
▬	Han et al. 45deg V-Down[1]	1	45	10	0.0625	Continuous rib
*	Han et al. 45deg[1]	1	45	10	0.0625	Continuous rib
◇	Taslim et al. 45deg V-UP[2]	1	45	10	0.083	Continuous rib
+	Taslim et al. 45deg V-Down[2]	1	45	10	0.083	Continuous rib
□	Taslim et al. 45deg[2]	1	45	10	0.083	Continuous rib
△	Taslim et al. V Discrete[2]	1	45	10	0.083	Discrete rib
I	Cho et al. [3]	2	45	10	0.1	Discrete rib
×	Gao & Sunden 60deg V-up[4]	8	60	10	0.1	Continuous rib
○	Gao & Sunden 60deg V-down[3]	8	60	10	0.1	Continuous rib
□	Gao & Sunden 60deg[4]	8	60	10	0.1	Continuous rib
II	Mahmood et al.[7]	16		8	0.4	Dimpled surface
⊕	Won et al.[11]	8		2		Pin fins
#	Dutta & Hossain[12]	5	5	6.35		Perforated baffle
●	Chang et al. forward flow[19]	8		10	0.1	Scaled surface
▲	Chang et al. backward flow[19]	8		10	0.1	Scaled surface
★	Chang et al. [22]	tube		10		Serrated Twisted-tape (twist ratio=1.56)

Fig. 4. Comparison of present Nusselt number ratios ($(\overline{Nu}/Nu_\infty)$ with varieties of HTE devices.

Fig. 5a. Fanning friction factors for the present test channel with forward flows constantly operate at the lower levels than the backward-flow counterparts. This result agrees with our previous work that examined the variations of Fanning friction factor against Re in the scale-roughened channel [19]. In the range of $1000 \leqslant Re \leqslant 30{,}000$, Fanning frictions factors in the present test channel with forward and backward flows are, respectively, correlated as

$$C_f = 17.098 \times Re^{-0.449} \quad \text{(forward flow)} \tag{11}$$

$$C_f = 17.17 \times Re^{-0.5} \quad \text{(backward flow)} \tag{12}$$

Augmentations of friction factor from the smooth-walled tube levels for the present compound HTE roughness are indexed by the $C_f/C_{f\infty}$ ratios. Fig. 5b plots the variations of $C_f/C_{f\infty}$ ratio against Re for forward and backward flows in which the $C_f/C_{f\infty}$ data reported for varieties of single and compound HTE measures are included for comparison. The $C_f/C_{f\infty}$ ratios for the present test channel and the scaled roughened channel of $H/W = 1/8$ [19] are among the highest magnitudes between the comparative groups collected in Fig. 5b. In the present test channel of aspect ratio $(H/W) = 1/2$, the compound surface roughness that consolidates protruding V-ribs and deepened scales constantly exhibits the higher $C_f/C_{f\infty}$ ratios than those counterparts in the scale roughened channel of $H/W = 1/8$ due to the additional pressure drops induced by V-ribs. Ratios of $C_f/C_{f\infty}$ for the present forward and backward flows also decrease with the increase of Re which fall, respectively, in the ranges of 32.4–16.8 and 46.7–27.7. The significant HTE impacts observed in Fig. 4 for the present test channel are accompanying with the high pressure drop

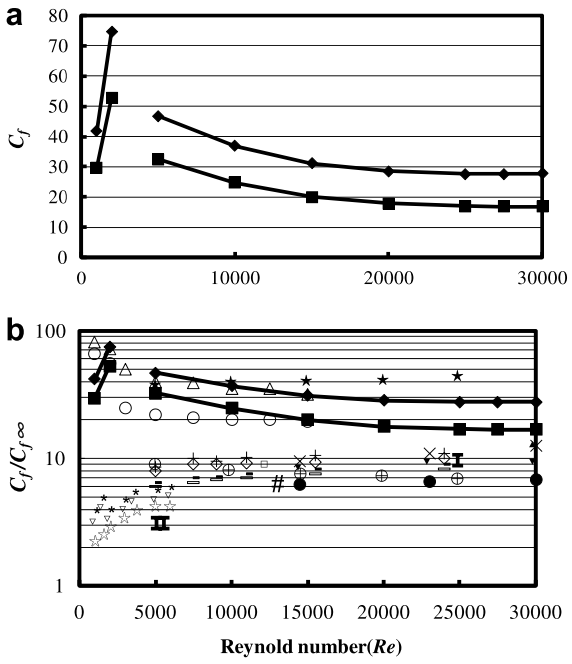

Symbol	References	(H/W)	α^R	Pitch ratio	e/H	HTE device
◆	Forward flow (present study)	2	45	10	0.044	V-rib Scaled surface
■	backward flow(present study)	2	45	10	0.044	V-rib Scaled surface
▼	Han et al. 45deg V-up[1]	1	45	10	0.0625	Continuous rib
▬	Han et al. 45deg V-Down[1]	1	45	10	0.0625	Continuous rib
*	Han et al. 45deg[1]	1	45	10	0.0625	Continuous rib
◇	Taslim et al. 45deg V-UP[2]	1	45	10	0.083	Continuous rib
+	Taslim et al. 45deg V-Down[2]	1	45	10	0.083	Continuous rib
□	Taslim et al. 45deg[2]	1	45	10	0.083	Continuous rib
△	Taslim et al. V Discrete[2]	1	45	10	0.083	Discrete rib
I	Cho et al.[3]	16		8	0.4	Dimpled surface
×	Gao & Sunden 60deg V-up[4]	8	60	10	0.1	Continuous rib
○	Gao & Sunden 60deg V-down[4]	8	60	10	0.1	Continuous rib
□	Gao & Sunden 60deg[4]	8	60	10	0.1	Continuous rib
II	Olsson & Sunden.[8]	16		8	0.4	Dimpled surface
#	Dutta & Hossain[12]	5	5	6.35		Perforated baffle
●	Chang et al. Forward flow[19]	8		10	0.1	Scaled surface
▲	Chang et al. backward flow[19]	8		10	0.1	Scaled surface
★	Chang et al. [22]	tube		10		Serrated Twisted-tape (twist ratio=1.56)

Fig. 5. Comparison of present pressure-drop performances with varieties of HTE devices.

penalty. This result has led to the requirement for comparing the thermal performance factors (η) between varieties of HTE measures. But for the engineering applications that request very high HTE effects with the Nu levels about 6 times of Nu_∞, the high pressure drops incurred by the present compound HTE roughness must be compensated.

3.3. Thermal performance factors

Fig. 6 shows the comparison of thermal performance factors of present compound HTE device with varieties of single and compound HTE measures. It is a common trend that the thermal performance factors (η) decrease as Re increases for turbulent flows. The descending rates of η versus Re curves vary with the HTE measures adopted. In general, the ribbed channel, twisted-tape insert and inclined perforated baffle exhibit the faster descending rates of η curves as shown in Fig. 6 so that the thermal performances with cooling applications involving high Reynolds numbers are deteriorated for these types of HTE measures. But the present compound HTE device and the scale-roughened channel [19] offer the relatively steady thermal performances as Re increases. These favorable data trends are attributed from the steady performance of HTE

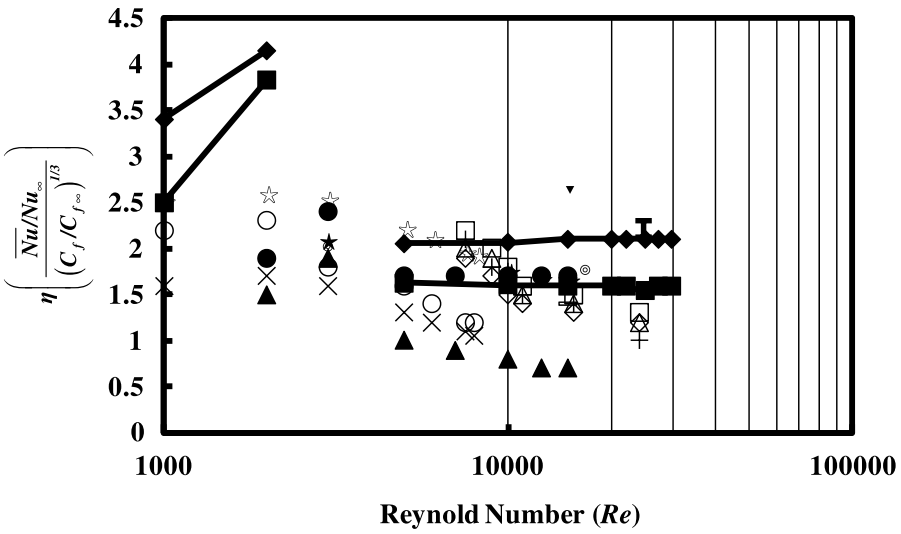

Symbols	References	Channel aspect ratio	α^R	Pitch ratio	e/H	HTE device
◆	Forward flow (present study)	2	45	10	0.044	V-rib Scaled surface
■	backward flow(present study)	2	45	10	0.044	V-rib Scaled surface
▾	Han et al. 45deg V-up[1]	1	45	10	0.0625	Continuous rib
▬	Han et al. 45deg V-Down[1]	1	45	10	0.0625	Continuous rib
⋆	Han et al. 45deg[1]	1	45	10	0.0625	Continuous rib
◇	Taslim et al. 45deg V-UP[2]	1	45	10	0.083	Continuous rib
+	Taslim et al. 45deg V-Down[2]	1	45	10	0.083	Continuous rib
□	Taslim et al. 45deg[2]	1	45	10	0.083	Continuous rib
△	Taslim et al. V Discrete[2]	1	45	10	0.083	Discrete rib
I	Cho et al.[3]	16		8	0.4	Dimpled surface
×	Gao & Sunden 60deg V-up[4]	8	60	10	0.1	Continuous rib
○	Gao & Sunden 60deg V-down[4]	8	60	10	0.1	Continuous rib
▯	Gao & Sunden 60deg[4]	8	60	10	0.1	Continuous rib
#	Dutta & Hossain[12]	5	5	6.35		Perforated baffle
◎	Chang et al.[16]	tube				Triple twisted-tape (twist ratio=1.67)
●	Chang et al. Forward flow[19]	8		10	0.1	Scaled surface
▲	Chang et al. backward flow[19]	8		10	0.1	Scaled surface
★	Chang et al. [22]	tube		10		Serrated Twisted-tape (twist ratio=1.56)

Fig. 6. Comparison of present thermal performance factors with varieties of HTE devices.

impacts for turbulent flows as demonstrated in Fig. 4. With laminar flows, the thermal performance factors in present test channel and the scale-roughened channel [19] increase as Re increases. This particular data trend reverses the typical results found in the rib-roughened channels and demonstrates the superiority of present compound HTE roughness in thermal performances for laminar flows. With $Re < 3000$, thermal performance factors for the present forward and backward flows are considerably higher than the comparative groups shown in Fig. 6. Once again, the thermal performance factors for the present compound HTE roughness with forward turbulent flows score the highest values among the various single and compound HTE measures compared in Fig. 6. Even for the backward flows with $Re > 20{,}000$, the η values are higher than those developed in the channel fitted with discrete ribs. In view of the comparative results depicted in Figs. 4 and 6, the present compound HTE roughness with forward flows simultaneously offer the highest values of $\overline{Nu}/Nu_\infty$ and η that is suitable for cooling applications of gas turbine blades for which the structure integrity of the roughness itself is satisfied.

4. Conclusions

A novel compound HTE roughness that consolidates the deepened scales and protruding V-ribs is developed. In the range of $1000 \leqslant Re \leqslant 30{,}000$, the performances of heat transfer and pressure drop in a rectangular channel roughened by this compound HTE surface with bulk flows directed in the forward and backward directions are

examined. HTE impacts indexed by $\overline{Nu}/Nu_\infty$ ratios for forward and backward flows are, respectively, in the ranges of 9.5–13.6 and 9–12.3 with laminar flows and 6.8–6.3 and 5.7–4.3 with turbulent flows. The $\overline{Nu}/Nu_\infty$ ratio of 6.8 at $Re = 30{,}000$ in the present test channel with forward flow soars the highest level among the varieties of single and compound HTE devices available to date. The weighted Re impacts on $\overline{Nu}$ for the present compound HTE roughness considerably extend the effective Re range for heat transfer augmentations. Structural integrities of this compound HTE surface are satisfied with cooling applications to gas turbine blades. HTE impacts offered by this compound HTE roughness are accompanied by high pressure drop penalties with the $C_f/C_{f\infty}$ ratios reaching about 24 and 37 for turbulent forward and backward flows, respectively. But the significant HTE effects offset the pressure drop penalties that considerably elevate the thermal performance factors in the test channel roughened by scales and V-ribs. Ratios of $\overline{Nu}/Nu_\infty$ and thermal performance factor in the present test channel with forward turbulent flows score the highest values among the varieties of single and compound HTE devices [1–19,21,22]. Empirical correlations of $\overline{Nu}$ and C_f with Re as the determined variable are developed for design applications.

References

[1] J.C. Han, Y.M. Zhang, C.P. Lee, Augmented heat transfer in square channels with parallel, crossed, and V-shaped angled ribs, ASME J. Turbomach. 113 (1991) 590–597.

[2] M.E. Taslim, T. Li, D. Kercher, Experimental heat transfer and friction in channels roughened with angle, V-shaped, and discrete ribs on two opposite walls, ASME J. Turbomach. 118 (1996) 20–28.

[3] H.H. Cho, S.J. Wu, H.J. Kwon, Local heat/mass transfer measurement in a rectangular duct with discrete ribs, ASME J. Turbomach. 122 (2000) 579–586.

[4] X. Gao, B. Sundén, Heat transfer and pressure drop measurements in rib-roughened rectangular ducts, Exp. Therm. Fluid Sci. 24 (2001) 25–34.

[5] X. Gao, B. Sundén, PIV measurement of the flow field in rectangular ducts with 60° parallel, crossed and V-shaped ribs, Exp. Therm. Fluid Sci. 28 (2004) 639–653.

[6] R. Kiml, A. Magda, S. Mochizuki, A. Murata, Rib-induced secondary flow effects on local circumferential heat transfer distribution inside a circular rib-roughened tube, Int. J. Heat Mass Transfer 47 (2004) 1403–1412.

[7] G.I. Mahmood, M.L. Hill, D.L. Nelson, P.M. Ligrani, H.-K. Moon, B. Glezer, Local heat transfer and flow structure on and above a dimpled surface in channel, ASME J. Turbomach. 123 (2001) 115–123.

[8] C.-O. Olsson, B. Sundén, Heat transfer and pressure drop characteristics of ten radiator tubes, Int. J. Heat Mass Transfer 39 (1996) 3211–3220.

[9] G.I. Mahmood, P.M. Ligrani, Heat transfer in a dimpled channel: combined influences of aspect ratio, temperature ratio, Reynolds number, and flow structure, Int. J. Heat Mass Transfer 45 (2002) 2011–2020.

[10] M.K. Chyu, Y.C. Hsing, V. Natarajan, Convective heat transfer of cubic fin arrays in a narrow channel, ASME J. Turbomach. 120 (1998) 362–367.

[11] S.Y. Won, G.I. Mahmood, P.M. Ligrani, Spatially-resolved heat transfer and flow structure in a rectangular channel with pin fins, Int. J. Heat Mass Transfer 47 (2004) 1731–1743.

[12] P. Dutta, A. Hossain, Internal cooling augmentation in rectangular channel using two inclined baffles, Int. J. Heat Fluid Flow 26 (2005) 223–232.

[13] R.M. Manglik, A.E. Bergles, Heat transfer and pressure drop correlations for twisted tape inserts in isothermal tubes: Part II – transition and turbulent flows, ASME J. Heat Transfer 115 (1993) 890–896.

[14] L. Wang, B. Sundén, Performance comparison of some tube inserts, Int. Comm. Heat Mass Transfer 29 (2002) 45–56.

[15] S. Martemianov, V.L. Okulov, On heat transfer enhancement in swirl pipe flows, Int. J. Heat Mass Transfer 47 (2004) 2379–2393.

[16] S.W. Chang, K.W. Yu, M.H. Lu, Heat transfer in tubes fitted with single, twin and triple twisted tapes, J. Exp. Heat Transfer 18 (2005) 279–294.

[17] St. Tiggelbeck, N.K. Mitra, M. Fiebig, Experimental investigations of heat transfer enhancement and flow losses in a channel with double rows of longitudinal vortex generators, Int. J. Heat Mass Transfer 36 (1993) 2327–2337.

[18] J.X. Zhu, M. Fiebig, N.K. Mitra, Numerical investigation of turbulent flows and heat transfer in a rib-roughened channel with longitudinal vortex generators, Int. J. Heat Mass Transfer 38 (1995) 495–501.

[19] S.W. Chang, T.-M. Liou, M.H. Lu, Heat transfer of rectangular narrow channel with two opposite scale-roughened walls, Int. J. Heat Mass Transfer 48 (2005) 3921–3931.

[20] F.W. Dittus, L.M.K. Boelter, University of California, Berkeley, CA, Publications in Engineering, vol. 2, 1930, p. 443.

[21] V. Zimparov, Enhancement of heat transfer by a combination of a single start spirally corrugated tubes with a twisted tape, Exp. Therm. Fluid Sci. 25 (2002) 535–546.

[22] S.W. Chang, Y.J. Jan, J.S. Liou, Turbulent heat transfer and pressure drop in tube fitted with serrated twisted tape, Int. J. Therm. Sci. 46 (2006) 506–518, 2007.

[23] JHT Editorial Board of ASME J. Heat Transfer, Journal of Heat Transfer Policy on Reporting Uncertainties in Experimental Measurements and Results, ASME J. Heat Transfer 115 (1993) 5–6.